



Assessment of variability of the thermohaline structure and transport of Atlantic water in the Arctic Ocean based on NABOS CTD data

Nataliya Zhurbas¹ and Natalia Kuzmina¹

¹Shirshov Institute of Oceanology, Russian Academy of Sciences, 36 Nakhimovsky Prospekt, 117997
5 Moscow, Russia

Correspondence to: Nataliya Zhurbas (nvzhurbas@gmail.com)

Abstract. Data of CTD transects across continental slope of the Eurasian Basin and the St. Anna Trough performed during NABOS (Nansen and Amundsen Basins Observing System) project in 2003–2015 are used to assess transport and propagation features of the Atlantic Water (AW) in the Arctic
10 Ocean. Estimates of θ - S indices and volume flow rate of the current carrying the AW in the Eurasian Basin were obtained. The assessments were based on the analysis of CTD data including 33 sections in the Eurasian Basin, 4 transects in the St. Anna Trough and 2 transects in the Makarov Basin; additionally a CTD transect of the PolarStern-1996 expedition (PS-96) was considered. Using spatial
15 distributions of temperature, salinity, and density on the transects and applying θ - S analysis, the variability of thermohaline pattern on the AW pathway along the slope of Eurasian Basin was investigated. The Fram Strait branch of the Atlantic Water (FSBW) was satisfactorily identified on all transects, including two transects in the Makarov Basin (along 159°E), while the cold waters, which can be associated with the influence of the Barents Sea branch of the Atlantic water (BSBW), on the transects along 126°E, 142°E and 159°E, were observed in the depth range below 800 m and had a
20 negligible effect on the spatial structure of isopycnic surfaces. Special attention was paid to the variability of the volume flow rate of the AW propagating along the continental slope of the Eurasian Basin. The geostrophic volume flow rate was calculated using the dynamic method. An interpretation of the spatial and temporal variability of hydrological parameters characterizing the flow of the AW in the Eurasian Basin is presented. The geostrophic volume flow rate decreases significantly farther away
25 from the areas of the AW inflow to the Eurasian Basin. Thus, the geostrophic estimate of the volume rate for the AW flow in the Makarov Basin at 159°E was found to be more than an order of magnitude smaller than the estimates of the volume flow rate in the Eurasian Basin, implying that the major part of



the AW entering the Arctic Ocean circulates cyclonically within the Nansen and Amundsen Basins. There is an absolute maximum of θ_{max} (AW core temperature) in 2006–2008 time series and a maximum in 2013, but only at 103°E. Salinity $S(\theta_{max})$ (AW core salinity) time series display an increase of the AW salinity in 2006–2008 and 2013 (at 103°E) that can be referred to as a AW salinization in the early 2000-ies. The maxima of θ_{max} and $S(\theta_{max})$ in 2006-2008 and 2013 were accompanied by the volume flow rate highs. Additionally the time average volume rates were calculated for the FSBW flow (in the longitude range 31–92°E), for the BSBW flow in the St. Anna Trough and for a combined FSBW and BSBW flow in longitude range 94–107°E. A detailed discussion of the results is presented.

1 Introduction

It is well known (see, e.g., Aagaard, 1981; Rudels et al., 1994; Schauer et al., 1997; Rudels et al., 1999; Schauer et al., 2002; Rudels et al., 2006; Berzczynska-Möller et al., 2012; Rudels et al., 2015; Rudels, 2015; Dmitrenko et al., 2015) that Atlantic water (AW) enters the Eurasian Basin in two ways: one part originates from the Greenland and Norwegian seas and flows to the Basin through the Fram Strait (Fram Strait branch of the Atlantic Water, hereinafter the FSBW in accordance with the terminology of the paper by Schauer et al. (1997)), and the other reaches the deep part of the Arctic Ocean near St. Anna Through after passing through the Barents Sea (Barents Sea branch of the Atlantic water, hereinafter the BSBW as in (Schauer et al., 1997)). After entering the Eurasian Basin the FSBW forms an eastward subsurface baroclinic boundary current with a core of increased temperature and salinity adjacent to the continental slope. In the longitude range of 80–90°E it encounters and partially mixes with the BSBW, which is strongly cooled due to mixing with shallow waters of the Arctic shelf seas. Further, the water masses resulting from the interaction of two branches which transport the AW continue spreading cyclonically in the Eurasian Basin, following the sea bed topography.

To study the characteristics of the FSBW and BSBW flow in the Eurasian Basin, it is useful to estimate, first of all, its volume flow rate in different parts of the Basin. Generally the estimates of the AW volume flow rate have been based on observationally derived velocities (Fahrbach et al., 2001; Pnyushkov et al., 2011; Berzczynska-Möller et al., 2012; Rudels et al., 2014). However, to solve a number of fundamental and climatic problems it is worth considering the AW volume flow rate



55 calculated on the basis of geostrophic (density-driven) velocity estimates. Such estimates can be more
close to the real average estimates of the baroclinic volume flow rate since the velocity field in the
ocean, in particular due to the internal waves and inertial oscillations, is usually more variable than the
temperature, salinity and density fields.

To estimate the volume flow rate and thermohaline parameters of the AW, a large amount of CTD
60 data is required. Obviously, the more complete the set of the considered sections the more accurate
would be the estimates. Within the NABOS project (Nansen and Amundsen Basins Observing System)
a unique array of CTD data was collected: more than 30 sections were made in various regions of the
Arctic Basin in the years 2002–2015. Moreover, a number of sections in different years were made in
the same regions of the Basin, which allows studying the temporal interannual variability of the
65 thermohaline structure of water masses in these areas.

The main goal of this work is to investigate the spatial and temporal variability of the AW volume
flow rate during its propagation along the continental slope of the Eurasian Basin using geostrophic
estimates. Another important aspect of our analysis is the investigation of the thermohaline structure of
the FSBW and BSBW and of its transformation. Large array of CTD data obtained using the NABOS
70 program in 2002–2015 is used to get the results.

2 Material and Methods

In this study we used data of CTD profiling on transects across the slope of the Eurasian Basin in
the longitude range of 31–159°E measured in the years 2002–2015 within the framework of NABOS
project (in total 39 transects). The data are freely available at the site <http://nabos.iarc.uaf.edu>. Apart
75 from the NABOS data, a famous CTD transect across the whole Eurasian Basin and over the
Lomonosov Ridge starting at 92°E at the slope from R/V *Polarstern* in 1996 (hereafter PS-96) was also
included. The location of the CTD transects is shown in Fig. 1. It can be seen from the map in Fig. 1
that most of the CTD transects are aligned cross-slope and grouped at longitudes of 31, 60, 90, 92, 94,
96, 98, 103, 126, 142, and 159°E. Four of the 40 transects crossed zonally the St. Anna Trough (at the
80 latitude of 81, 81.33, 81.42, and 82°N) through which the Barents Sea Branch of the Atlantic Water
(BSBW) enters the Eurasian Basin. Most of the CTD casts covered the upper layer from the sea surface



85

to either 1000 m depth or to the bottom (if the depth of the sea was less than 1000 m); some of the CTD casts (approximately every third or fourth) covered the depths from the sea surface down to the sea bottom even if the sea depth exceeded 1000 m.

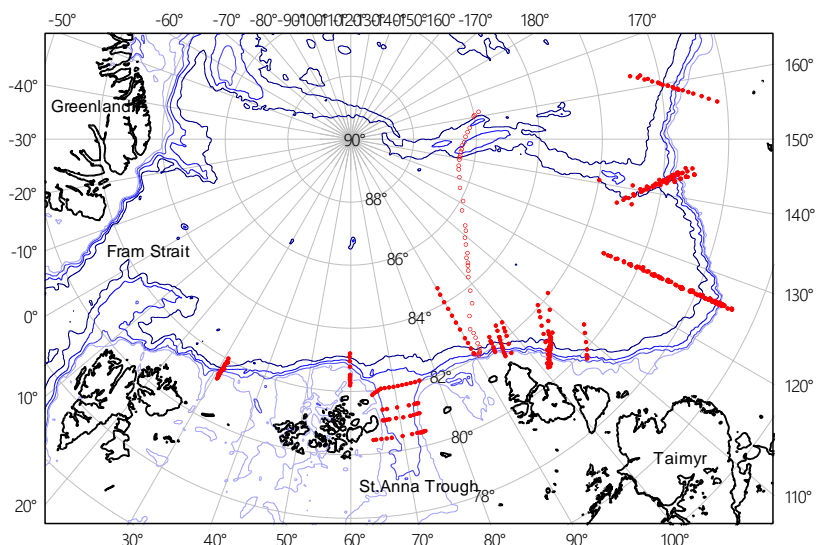


Fig. 1. Bathymetric map of the Eurasian Basin with 300, 500, 1000, and 2000 m contours shown. The red filled and blank circles are the locations of CTD stations on the NABOS and PS-96 transects, respectively.

90 To estimate the strength of the Fram Strait branch (FSBW) or the Barents Sea branch (BSBW) or both branches of the Atlantic Water, we applied classical geostrophic relations

$$\frac{\partial u}{\partial z} = \frac{g}{f \rho_0} \frac{\partial \rho}{\partial y}, \quad \frac{\partial v}{\partial z} = -\frac{g}{f \rho_0} \frac{\partial \rho}{\partial x}, \quad (1)$$

where u and v are velocity components along the x and y axes, respectively, g is the gravity acceleration, f is the Coriolis parameter, and ρ and ρ_0 are the density and reference density, respectively; x, y, z is the right-hand triplet of orthogonal axes (e.g., the $x, y,$ and z axes are directed east, north, and upward, respectively).

95



100

The choice of such a coordinate system is convenient for the stated task. Indeed, assuming that the direction of the flow which transports AW is perpendicular to the transects (that is, the flow is directed strictly along the slope), the first equation of Eqs. (1) was used to calculate the flow velocity in the Eurasian basin. The second equation of Eqs. (1) was used to estimate the flow velocity in the St. Anna Trough.

The horizontal gradients of density, $\partial\rho/\partial x$ or $\partial\rho/\partial y$, can be estimated from CTD measurements (non-averaged data) on the transect providing the possibility to calculate vertical gradients of velocity, $\partial v/\partial z$ or $\partial u/\partial z$ by Eqs. (1) and finally assess velocities u and v by vertical integration.

105

The main problem with geostrophic estimates of velocity from CTD transects lies in the uncertainty of choice of the no motion level (the zero velocity depth or the reference horizon). If one expects that the baroclinic current occupies the upper layer or/and some intermediate layer while the deep layer is relatively calm, the no motion depth level (or the reference horizon) can be chosen somewhere in a supposedly calm deep layer (where the horizontal density gradient is very small). On the contrary, in case of a near-bottom gravity flow, one would expect relative stillness in the overlying layers, so the no motion depth level can be reasonably chosen somewhere well above the near-bottom flow. The first situation is applicable to the FSBW, which is a near-surface current when entering the Eurasian Basin and is transformed to subsurface, intermediate-layer flow on its pathway along the slope of the Eurasian Basin. The latter situation is applicable to the BSBW in the St. Anna Trough. In view of the above considerations, we adopted for the no motion depth level either 1000 m depth or the sea bottom depth if the latter was smaller than 1000 m for the FSBW, and some level in the vicinity of 50 m depth, where density contours were more or less flat, for the observations of BSBW in the St. Anna Trough (see also below). An additional argument in favor of such a choice of the no motion depth level is that the CTD sections were made in the areas of Arctic Ocean covered with ice, and, consequently, the elevations of the free surface due to convergence/divergence caused by the heterogeneity of the Ekman wind transport, which could form the barotropic component of the geostrophic flow, are absent: the ice cover extent of all sections, except for the southernmost section in the Laptev Sea, at 126°E, was estimated to be about 95%.

110

115

120



Another problem with the geostrophic estimates of velocity from non-averaged CTD-data is
125 caused by vertical undulations of density contours on transect due to internal waves and mesoscale
eddies that can cause large fluctuations of horizontal density gradients and, therefore, unrealistically
high estimates of geostrophic velocities. The masking effect of internal waves and mesoscale eddies on
geostrophic estimates of velocity is especially important for transects with closely spaced CTD casts,
when the distance between neighbor casts is only a few kilometers (this is our case). However, the
130 masking effect of internal waves and mesoscale eddies can be suppressed by integrating geostrophic
velocities horizontally and vertically to get volume flow rate through the CTD transect. Indeed, to get
correct estimates of geostrophic velocities, it is better not to use non-averaged data: it is useful to
perform averaging and mapping the data on a regular grid. Selecting the optimal smoothing and regular
grid mapping parameters in each specific case of a CTD section to determine geostrophic current
135 velocities is beyond the scope of this paper: here we only present estimates of the volume flow rate
calculated on the basis of a formal approach to the analysis of non-averaged CTD data which excludes
the subjectivity of choice of averaging and mapping parameters.

Since the FSBW brings saline and warm water to the Eurasian Basin, the geostrophic estimates of
the volume flow rate were found by integration over the depth range with positive temperature, $\theta > 0$ °C,
140 and relatively high salinity, $S > 34.5$ psu, that is, some areas in the near-surface layer with warm and
fresh water (which cannot be attributed to AW) were excluded. For the observations of BSBW in the St.
Anna Trough the geostrophic estimates of the volume flow rate were found by integration over a depth
range with the non-averaged temperature below 0 °C and the salinity above 34.5 psu. If both branches
of AW were present on the transect, the integration was performed over the entire depth range except
145 the cold near-surface layer ($\theta < 0$ °C) and the areas in the near-surface layer with warm ($\theta > 0$ °C) and
relatively fresh ($S < 34.5$ psu) water. The zero velocity depth in this case was chosen in accordance to
the observed pattern of density contours, i.e. its resemblance with either the near-surface flow pattern or
the near-bottom flow pattern (see Section 3 for details). For density ρ in Eqs. (1), the in situ water
density depending on temperature, salinity and pressure was adopted. A detailed description of the
150 method for geostrophic estimates of the AW volume flow rate is presented in the paper (Zhurbas N.,
2019).



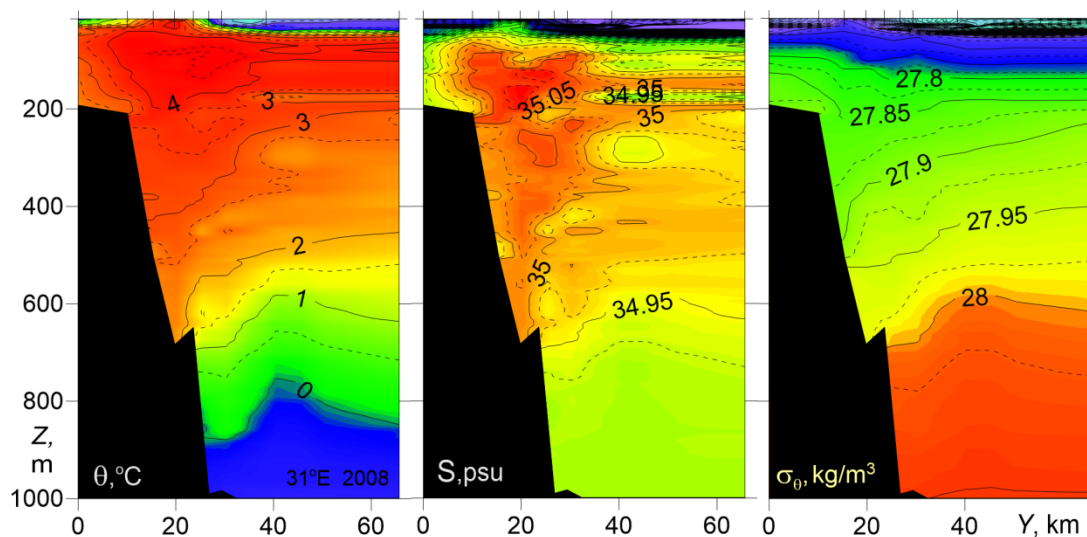
3 Results

3.1 Variability of the thermohaline pattern on the AW pathway along the slope of Eurasian Basin

3.1.1 CTD transections analysis

155 First of all, let us focus on the transformation of thermohaline signatures (i.e. patterns of salinity S , potential temperature θ , and potential density anomaly σ_θ , calculated relative to the atmospheric pressure $p_0 = 0$ dbar, versus cross-slope distance and depth) of the AW flow on its pathway along the slope of the Eurasian Basin. The potential density anomaly σ_θ pattern was of primarily interest, since it determines the geostrophic estimate of the AW transport (the values of hydrological parameters and
160 volume flow rates estimated for different areas of the AW flow based on empirical data are presented in the table in Section 3.2).

Fig. 2 shows temperature, salinity, and potential density anomaly versus cross-slope distance and depth from transect at 31°E, made in 2008. As it can be seen in Fig. 2, the contours of σ_θ diverge towards the continental slope margin (to the south), shallowing above the warm/saline core of the AW and sloping down beneath it, which in terms of geostrophic balance corresponds to the eastward
165 subsurface flow. Such a structural feature of the distribution of isopycnic surfaces was observed on all NABOS transects taken across available continental slope at 31°E. According to Fig. 2 the warm/saline core of the Fram Strait Branch of the AW with the maximum temperature θ_{max} of 4.88°C at the depth $Z_{\theta_{max}}=102$ m and the maximum salinity S_{max} of 35.11 psu at the depth $Z_{S_{max}}=176$ m is found on the
170 slope at about 1000 m isobath. It is obvious that the salinity maximum depth must be always larger than the temperature maximum depth to satisfy the condition of hydrostatic stability. Indeed, if $Z_{\theta_{max}}=Z_{S_{max}}$ then $\partial\sigma_\theta/\partial z = 0$ at $z = Z_{\theta_{max}} = Z_{S_{max}}$ (hydrostatically neutral stratification), and if $Z_{\theta_{max}} > Z_{S_{max}}$ then $\sigma_\theta(Z_{\theta_{max}}) < \sigma_\theta(Z_{S_{max}})$ (hydrostatically unstable stratification).



175 Fig. 2. Temperature θ , salinity S , and potential density anomaly σ_θ versus cross-slope distance and depth for the NABOS-08 transect across the Eurasian Basin slope at 31°E .

Fig. 3 presents temperature, salinity, and potential density versus distance and depth for two zonal transects across the St. Anna Trough at latitudes of 81 and 82°N . These transects presented in Fig. 3 are characterized by a stable pool of cold ($\theta < 0^\circ\text{C}$) and dense ($\sigma_\theta > 28 \text{ kg/m}^3$) water in the bottom layer adjacent to the eastern slope of the Trough. The transfer of the densest water pool to the eastern slope corresponds to a geostrophically balanced near-bottom gravity flow to the North. Note, that the gravity bottom currents are a typical feature of ocean dynamics and can develop in the narrows and troughs of various ocean basins (Arneborg et al., 2007; Zhurbas et al., 2012), so it is natural that the water flowing through St. Anna Trough in the Eurasian basin is transported by a gravity current. It is obvious that in case of near-bottom gravity current the no motion depth level for geostrophic calculations is implied to be well above the current. This near-bottom gravity current carries also waters of Atlantic origin, which are strongly cooled due to mixing with shallow waters of the Arctic shelf seas (the Barents and Kara seas). Above the near-bottom gravity flow of the BSBW one can observe two-core structure of warm FSBW with temperature up to 2.5°C that enters the St. Anna Trough from the north-west at the western side of the Trough and leaves it for the north-east at the eastern side of the Trough. At 82°N (top panels in Fig. 3), the BSBW overflows a sufficiently deep ridge (at approx. 500 m depth) between the St. Anna Trough and the Voronin Trough. The latter is located in the longitude range of 80 – 90°E east of the St.



195

Anna Tough and west of the Severnaya Zemlya islands (see Fig. 1). Therefore, one may suggest that a part of the BSBW enters the Eurasian Basin at 90°E leaving the Voronin Trough. See also (Schauer et al., 2002; Rudels et al., 2014).

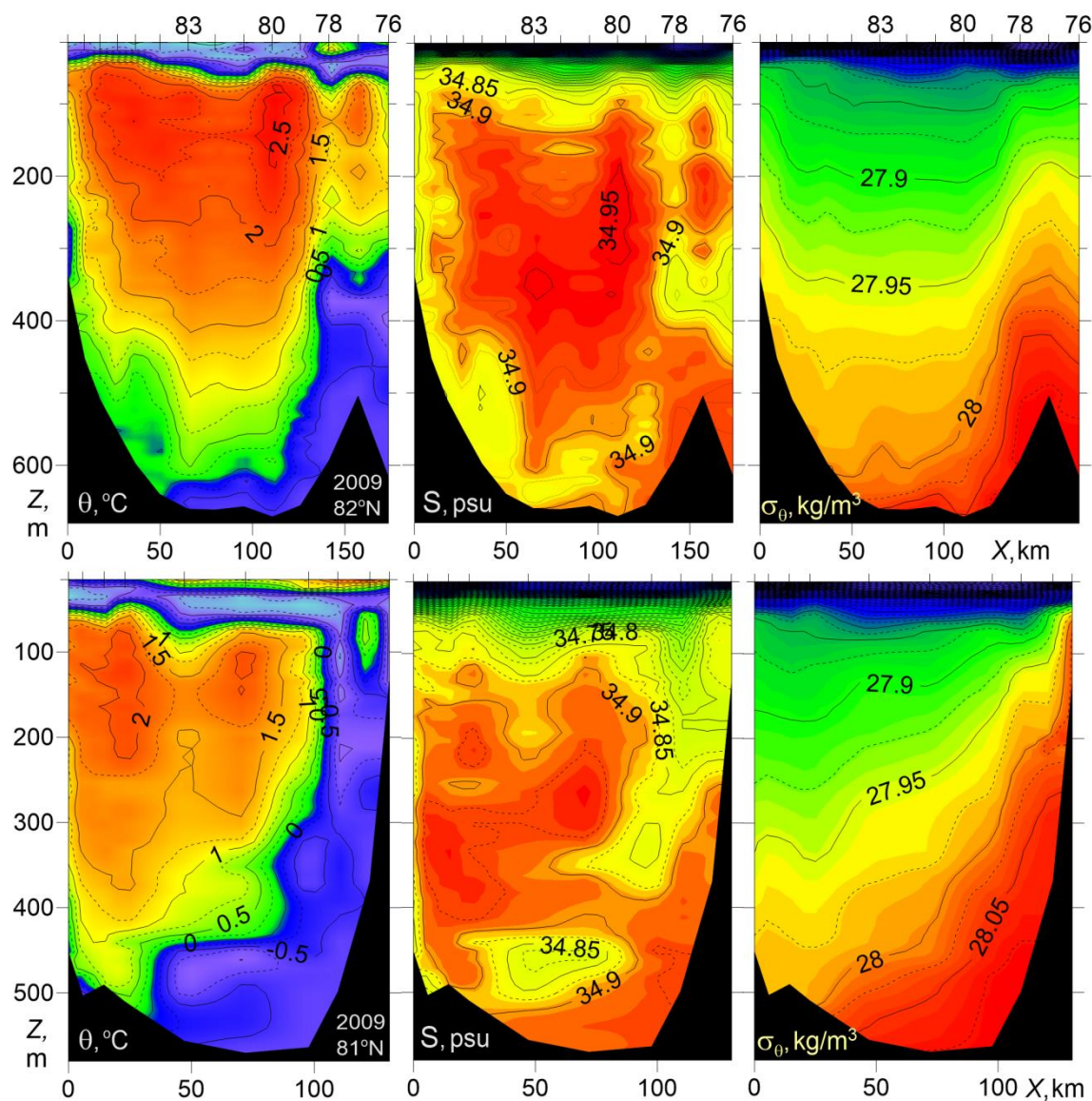


Fig. 3. Temperature θ , salinity S , and potential density anomaly σ_θ versus distance and depth for zonal transects across the St. Anna Trough at latitudes of 81°N (bottom, NABOS-09), and 82°N (top, NABOS-09). The X -axis is directed to the east.



200 To understand the mechanisms of interaction and transformation of the FSBW and the BSBW, it is necessary to identify water masses of different origin. For that purpose the following criterion is often used (Walsh et al., 2007; Pfirman et al., 1994): the water masses of the FSBW are characterized by $\theta > 0$ °C, and the BSBW can be identified by the following expressions: -2 °C $< \theta < 0$ °C, 34.75 psu $< S < 34.95$ psu and 27.8 kg/m³ $< \sigma_{\theta} < 28.0$ kg/m³. However, according to Fig. 3, the potential density σ_{θ} of the
205 BSBW exceeds the upper limit of the last inequality, reaching the value of 28.05 kg/m³ and the potential temperature θ does not reach the value of -2 °C and is less than -1 °C only in some cases. Thus, the BSBW thermohaline indices can be close to the values of temperature and salinity in the so-called Upper Polar Deep Water layer (UPDW, Rudels et al., 1994), the potential temperature of which lies within the range -0.5 °C $< \theta < 0$ °C, and the salinity is close to 34.9 psu (Walsh et al., 2007). Such a layer
210 can be seen in Fig 2 in the depth range below 800 m. The overlapping of the ranges of variability of temperature and salinity for the UPDW and the BSBW makes it difficult to determine the origin of water masses in the eastern part of the Nansen Basin. In some cases, however, analysis of θ - S diagrams can provide useful information for identification of different water masses (see Subsection 3.1.2).

In Fig. 4 the CTD transect at 92° E carried out in the *Polarstern*-1996 expedition just east of the
215 entrance point of the BSBW to the Eurasian Basin from the St. Anna Trough and Voronin Trough is presented. It can be assumed that a part of the BSBW extends deep into the Basin, mixing with the FSBW, while another part of the BSBW moves eastward along the slope as a deep gravity current according to the general cyclonic circulation observed in the Eurasian Basin. On the presented transect the BSBW is observed in the depth range below 600 m as a narrow, about 10 km wide stripe of cold
220 water near the slope (see also Subsection 3.1.2) adjacent to a 300 km wide zone occupied by the warm FSBW. The pattern of the potential density of FSBW on this transect is similar to transects at 31° E. Namely, despite of the masking effect of vertical undulations of σ_{θ} contours caused by internal waves and mesoscale eddies (one of subsurface, intra-pycnocline eddies is probably identified at the distance of $Y=510$ km), one cannot miss the tendency of shallowing/sloping down the σ_{θ} contours above/below
225 the FSBW core towards the continental slope margin (to the south) which, in terms of geostrophic balance implies the eastward flow of FSBW. The FSBW core on the 92° E transect is found at 40 km distance from the slope, with the maximum temperature $\theta_{max}=2.79^{\circ}$ C at $Z_{\theta_{max}}=271$ m and salinity

230 $S_{max}=34.97$ psu at $Z_{S_{max}}=329$ m. Therefore, the FSBW on its pathway along the slope of the Eurasian Basin from 31°E to 92°E has cooled, desalinated, sank and become denser by approx. 2°C , 0.1 psu, 150 m, and 0.1 kg/m^3 , respectively. Another significant feature seen in the PS-96 transect is an increased temperature pool in the layer of $180\text{--}300$ m at the distance of $Y=600\text{--}750$ km in the vicinity of the Lomonosov Ridge which can be attributed to the FSBW return flow cyclonically circulating around the Eurasian Basin. Note that the existence of return flow next to the Lomonosov Ridge is confirmed in terms of geostrophic balance by sloping down density contours towards Y -axis.

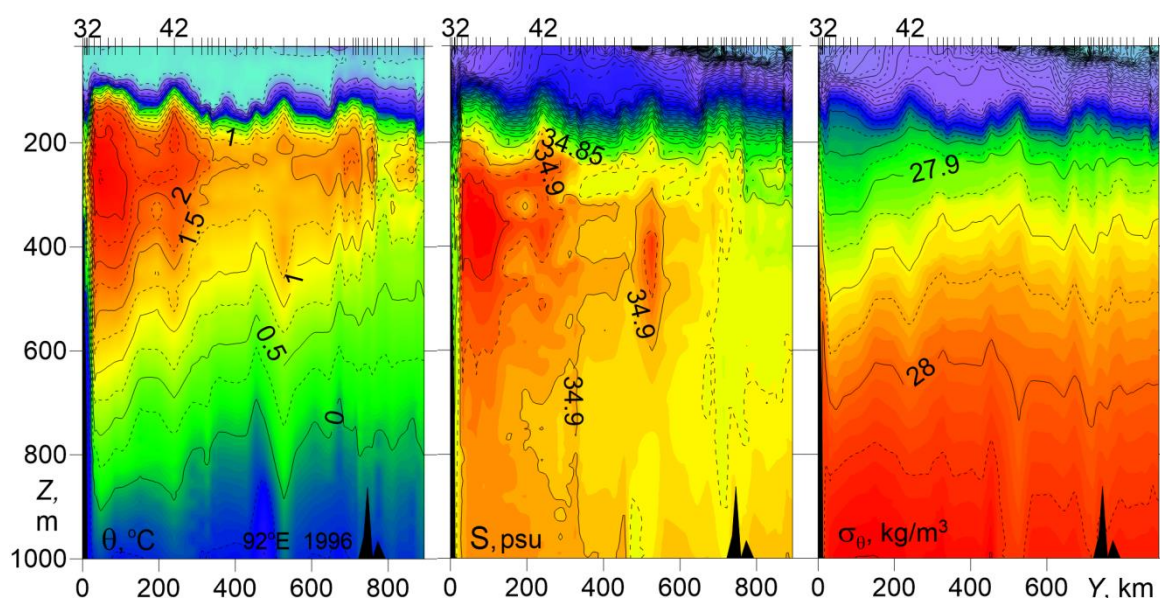
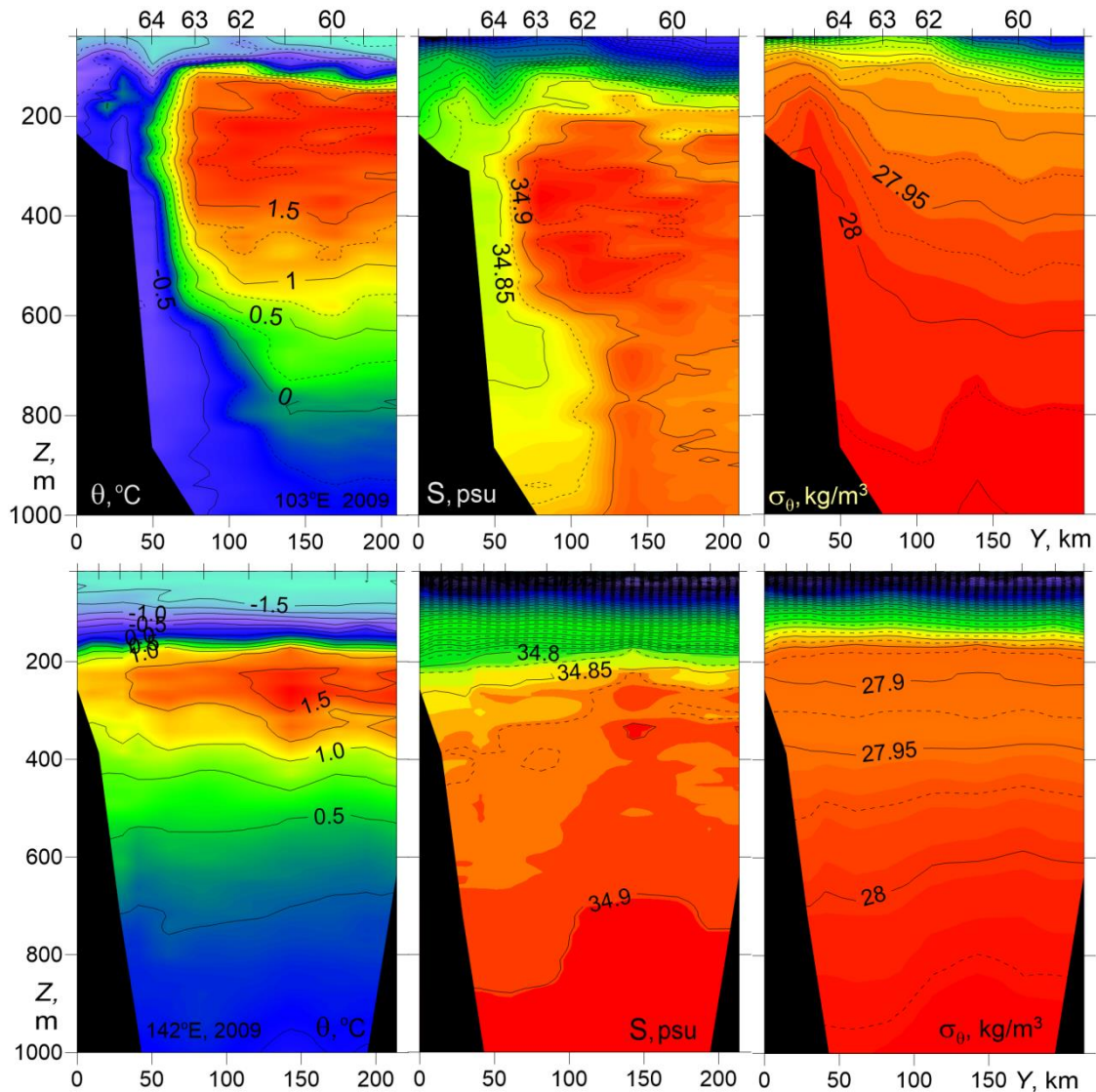


Fig. 4. Temperature θ , salinity S , and potential density anomaly σ_{θ} versus distance and depth for cross-shelf transects at 92°E (PS-96).

240 Further east, in the longitude range of $94\text{--}107^{\circ}\text{E}$ (NABOS-09), the BSBW being denser dives under the FSBW, and the pattern of potential density on cross-slope transects is characterized by sloping down density contours towards the North in a 150 km wide zone adjacent to the slope (see Fig. 5, top panel) which is typical for the near-bottom gravity currents and corresponds to the eastward geostrophic flow provided that the no motion depth level remains within the above-lying layers. One reason to associate the BSBW with gravity current is the potential temperature values below -0.5°C (see Subsection 3.1.2).



245

Fig. 5. Temperature θ , salinity S , and potential density anomaly σ_θ versus distance and depth for cross-shelf transects at 103°E (upper) and 142°E (lower) (NABOS-09).

The vertical location of the FSBW layer has not changed much relative to the 92°E in the section PS-96 but the maximum temperature has further decreased: in the transect in Fig. 5, the top panel, $\theta_{max}=1.98$ °C at $Z_{\theta_{max}}=245$ m and $S_{max}=34.95$ psu at $Z_{S_{max}}=365$ m. The bottom panel of Fig. 5 presents the data from transect at 142°E (NABOS-09) which is located on the Lomonosov Ridge, the frontier between the Amundsen and Makarov Basins. The comparison of the two transects obtained in the same

250



year shows that the vertical scale of the especially warm part of FSBW ($\theta > 1.5$ °C) has significantly decreased. Nevertheless, it is obvious that the FSBW is also observed at these latitudes and affect the slopes of isopycnic surfaces in a layer up to 300 m. The cold waters with $\theta < 0$ °C, which can be associated with the BSBW, are observed only at two stations in the depth range close to 1000 m, and are practically absent at the depths above 950 m. The slopes of isopycnic surfaces in the bottom panel of Fig. 5 are small, which is typical for weak geostrophic volume flow rate (see Section 3.2). It is worth noting that due to the low variability of the temperature and salinity fields, the water with absolutely stable thermohaline stratification is well visualized (Fig. 5, bottom panel): the temperature decreases and salinity increases with depth. This structural feature of the mean thermohaline stratification is also common to the UPDW (Rudels et al., 1999; Kuzmina et al., 2011, 2014).

In Fig. 6 three transects are presented, two of which were made at 126°E and 142°E (NABOS-05) and the third one was made in the Makarov Basin at 159° E (NABOS-07). On the transect along 126°E large slopes of isopycnic surfaces are observed, which corresponds to a fairly intensive geostrophic flow (see Section 3.2), confined to the depth range of 200–400 m, that is, to the area occupied by the FSBW. At the 142°E transect which is located on the Lomonosov Ridge, the frontier between the Amundsen and Makarov basins, and at the 159°E transect in the Makarov Basin, the FSBW can be still identified as a warm layer within a depth range of 200–400 m, where the maximum temperature has lowered to 1.49 °C and 1.42 °C, respectively (Fig. 6). One can observe some sloping down of potential density contours towards the continental slope on the 142°E transect implying some eastward geostrophic transport. As to the 159° E transect, the potential density contours look quite flat, so one cannot visually identify any significant baroclinic flow. In the area of cold waters (the depth range below 800 m) high slopes of isopycnic surfaces are not observed on any sections shown in Fig. 6, which may indicate the weakness or absence of the baroclinic flow.

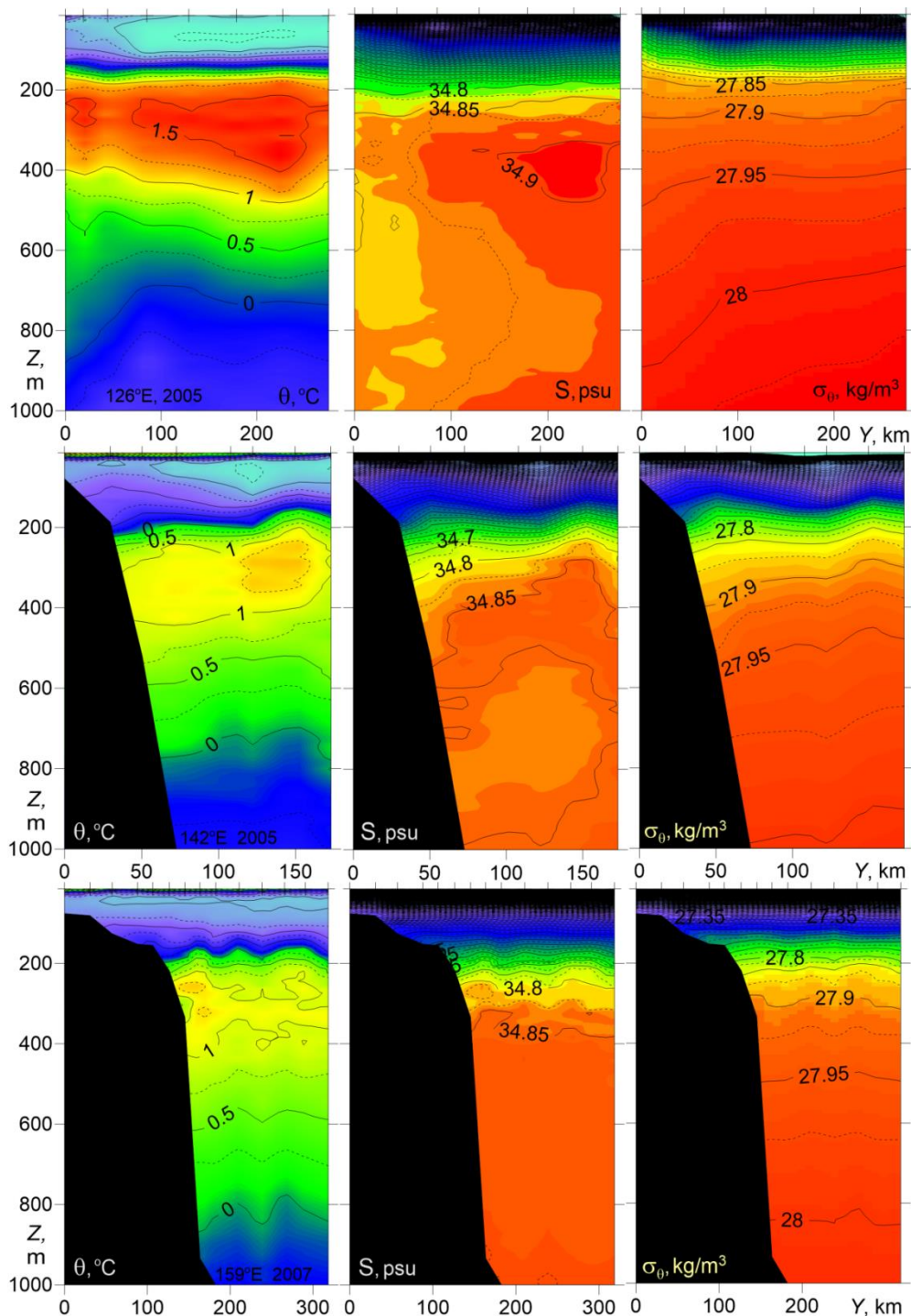


Fig. 6. Temperature θ , salinity S , and potential density anomaly σ_θ versus distance and depth for cross-shelf transects at 126°E, 142°E (top and middle, NABOS-05) and 159°E (bottom, NABOS-07).



280 Concluding this section, we would like to state the following theses. The combined FSBW-BSBW structure with isopycnals sloping down to the north (from the slope), is typical for the longitude range 94–107°E. On the transects made along 126°E, 142°E, and 159°E, the slopes of isopycnic surfaces indicating the baroclinic flow, were observed generally in the depth range of 200–400 m, that is in the area occupied by the FSBW. As the FSBW moved along the continental slope of the Eurasian Basin, a
285 significant decrease of temperature was observed in the FSBW core. However, despite this the FSBW was satisfactorily identified at all transects, including the two transects in the Makarov Basin (159°E). The cold waters on the transects along 126°E, 142°E and 159°E, which can be associated with the BSBW, had a minimum temperature above -0.5 °C, were observed in the depth range below 800 m and had a little effect on the spatial structure of isopycnic surfaces.

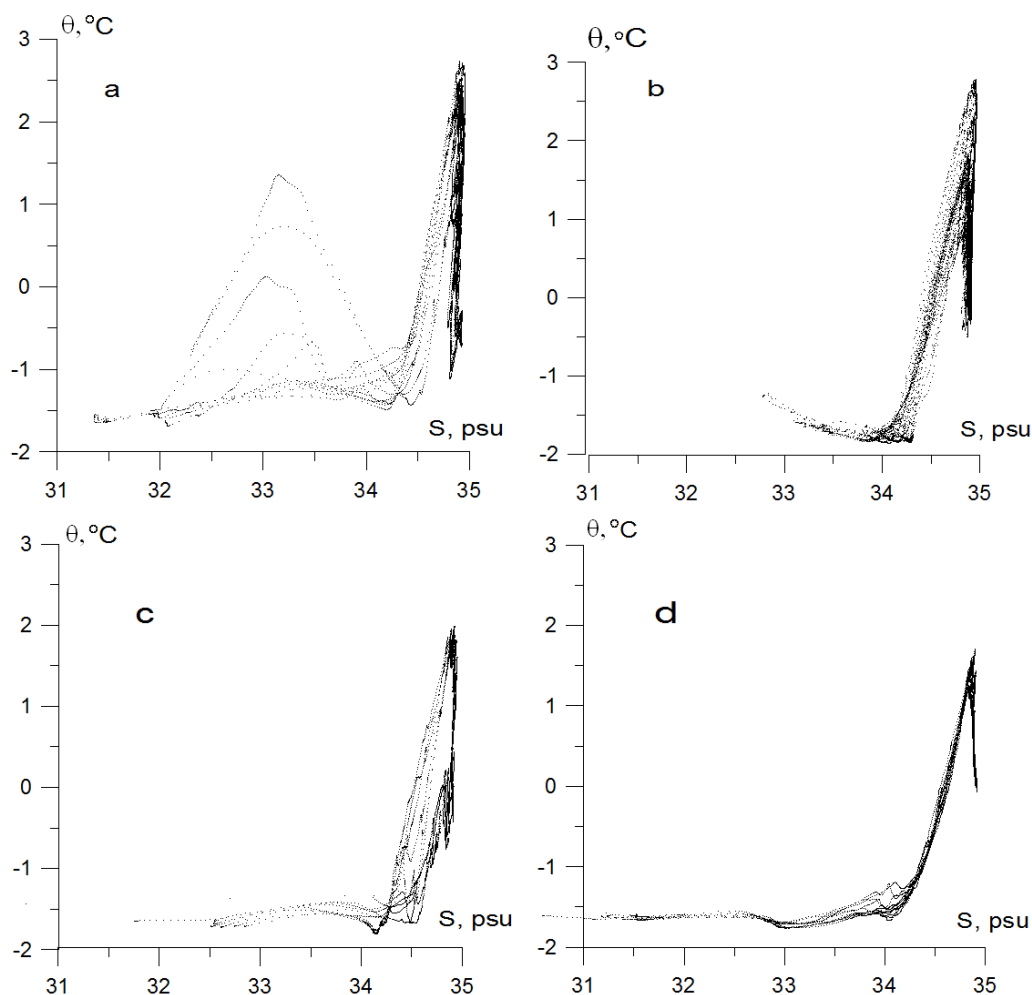
290 3.1.2 θ -S analysis

To study the transformation of various water masses in the Arctic Basin the θ -S analysis have been applied in a number of papers (see, e.g., Schauer et al., 1997; Rudels et al., 1999; Schauer et al., 2002; Rudels et al., 2004; Walsh et al., 2007; Dmitrenko et al., 2015). We will also apply this method to study the transformation of BSBW along the slope.

295 As mentioned above, the difficulty in identifying the BSBW in the eastern part of the Nansen Basin is related to the overlapping ranges of temperature and salinity inherent to the BSBW and the upper layer of the Polar Deep Water (UPDW). It is also important to note that the BSBW in the St. Anna Trough mixes with the FSBW. Therefore, not only the cold Atlantic Waters, which are transported by the bottom gravity current, but also mixed warmer waters can enter the Nansen Basin
300 through the Trough (see Fig. 3). That is, one can observe some resemblance in the potential temperature and salinity distributions across the St. Anna Trough (Fig. 3) and that of the cross-slope section PS-96 at 92°E (Fig. 4), despite of the fact that the CTD measurements were performed in different years. Therefore, it is expected that only a detailed analysis of the θ -S indices on different CTD sections, obtained at approximately the same time (e.g., the same year), can provide useful information on the
305 movement and transformation of BSBW.



Fig. 7 presents θ - S diagrams based on the CTD profiling in (a) the St. Anna and Voronin Troughs (NABOS-09, 82°N), (b) the PS-96 section at 92°E, and the NABOS-09 sections at 103°E (c) and 142°E (d). For convenience of presentation, the points of the θ - S curves with salinity below 30 psu were omitted.



310

Fig. 7. θ - S diagrams based on the CTD profiling in (a) the St. Anna and Voronin troughs (NABOS-09, 82° N), (b) the PS-96 section at 92°E, and the NABOS-09 sections at 103°E (c) and 142°E (d).

315

The diagrams presented in Fig. 7 have significant similarities and differences. The differences in the behavior of the θ - S indices are observed in the upper and deep layers of the Eurasian Basin and the St. Anna Trough. On the other hand, one cannot miss a similarity in the shape of the θ - S curves in the salinity range of 34.5–35.0 psu. The similarity is obviously caused by the presence of FSBW. The plots



in Fig. 7 demonstrate the transformation of the FSBW and BSBW moving along the continental slope of the Eurasian Basin. More detailed information on the BSBW transformation can be extracted from θ - S diagrams presented in Fig. 8.

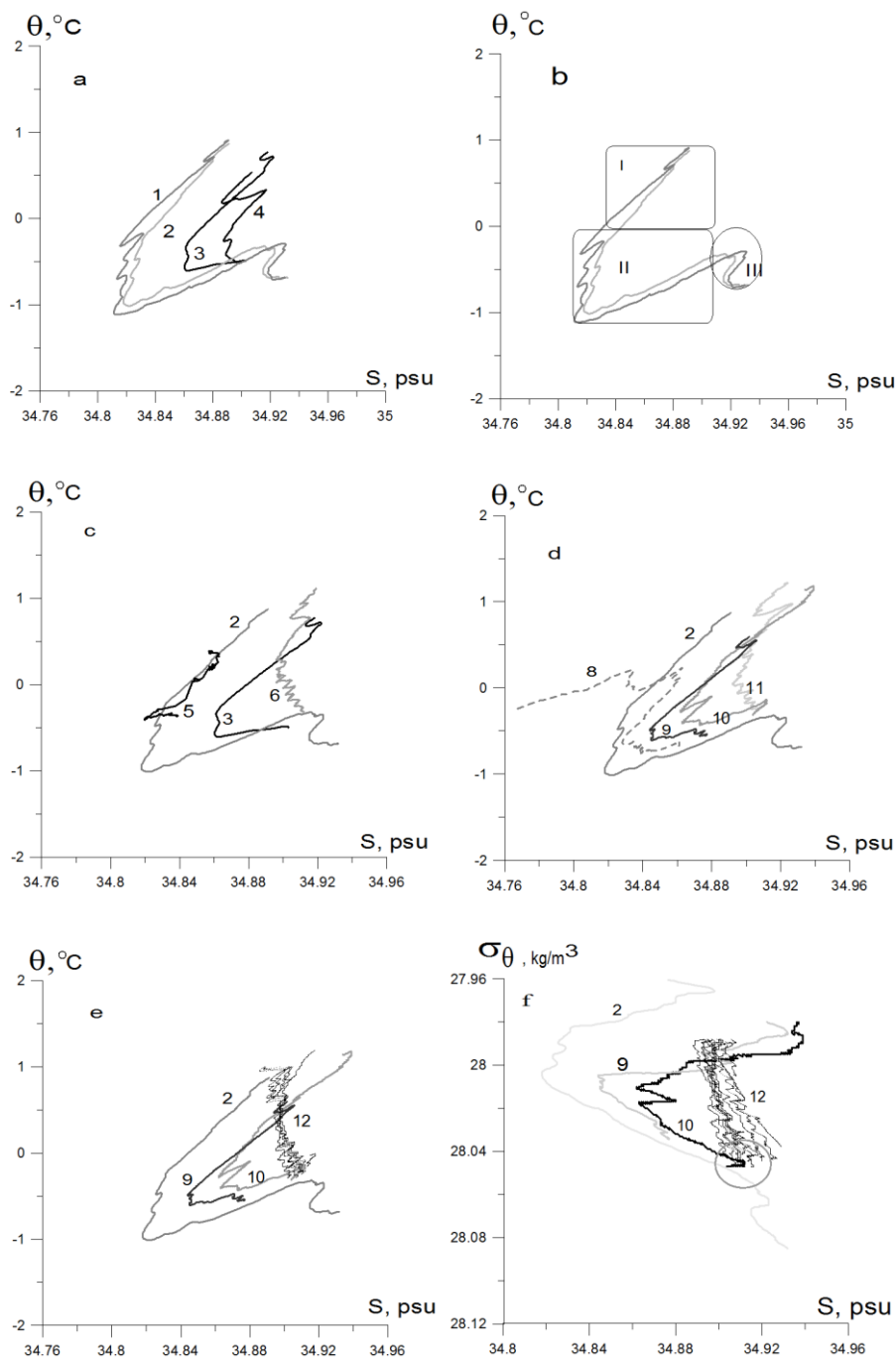




Fig. 8. Thermohaline indexes of the BSBW and FSBW: a) based upon the CTD profiles, obtained in the St. Anna Trough (NABOS-09, section 82°N), curves 1–4 correspond to the stations (st.) 76, 78, 83 and 80, respectively; b) the same as “a” but only curves 1 and 2 are presented; regions I, II, III illustrate three different water masses in accordance with (Dmitrenko et al., 2015); for explanation, see the text; 325 c) based upon the section of PS-96, curves 5 and 6 corresponding to st. 32 and 42, respectively (depth range 600–1000 m), curves 2 and 3 are shown for the reference; d) for CTD profiles at the 103°E section, NABOS-09, curve 8 (st. 64), curve 9 (st. 63), curve 10 (st. 62), curve 11 (st. 60), and curve 2 for the reference (see Fig. 5 for the location of the stations); e) based upon the CTD profiles in the depth range 500–1200 m measured at the 126°E (section of NABOS-09), curves 12; curves 2, 9 and 10 are 330 shown for the reference; f) the same as “e” but presented in coordinates σ_θ, S .

The θ - S diagrams related to the St. Anna Trough (NABOS-09, section 82°N) are presented in Fig. 8a. The curves marked as 1 and 2 correspond to stations 76 and 78, respectively, which were located at the eastern slope of the Trough just in the near-bottom gravity current carrying the BSBW, while the curves marked as 3 and 4 correspond to stations 83 and 80 located near the mid-point (thalweg) of the 335 Trough in the western periphery of the gravity current (the location of the stations is shown in Fig. 3). To visualize better the BSBW transformation, the points of θ - S curves in the temperature and salinity ranges of $\theta > 1.2$ °C and $S < 34.76$ psu, respectively, were omitted. The same kind of similarity of the θ - S curves in the St. Anna Trough was observed within NABOS Program in other years (NABOS-13, NABOS-15).

The curves 1 and 2 in Fig. 8a have similar knee-like shape (Dmitrenko et al., 2015) formed by (i) 340 the upper warm and saline water layer of the FSBW ($\theta \gg 0$ °C), (ii) the intermediate colder and fresher water layer of BSBW ($\theta < 0$ °C) underlying the FSBW, and (iii) the denser more warmer and saltier “true” mode of the BSBW ($\theta \approx 0$ °C). To understand better the differences between these water masses see Fig. 8b: FSBW (region I), BSBW (region II), “true” mode BSBW (region III). The difference 345 between the BSBW and “true” BSBW is in that the former is more diluted with the colder and fresher Barents Sea water (see paper by Dmitrenko et al. (2015) for more details). We will be interested in the transformation of the main part of the knee, namely the transformation of the moving along the slope BSBW.

In Fig. 8c the comparison of typical θ - S curves related to the St. Anna trough (they are also shown 350 in the other panels of Fig. 8 for reference) with that of the 92°E section of PS-96 is given: the curves 5



and 6 correspond to st. 32 and st. 42 (depth range 600–1000 m) of the PS-96 section, respectively. St. 32 was located next to the slope, while st. 42 was located about 250 km apart from the slope. The coincidence of curve 5 with a part of curve 2 evidences for the BSBW moving along the slope in the form of a near-bottom gravity flow (see Fig. 4 and its legend 1). Curve 6 corresponds to the UPDW.
355 The θ - S diagrams for CTD profiles at the section 103°E, NABOS-09, are given in Fig. 8d: curve 8 (st. 64), curve 9 (st. 63), curve 10 (st. 62), curve 11 (st. 60), and the reference curve 2 (see Fig. 5 for the location of stations). Curves 8, 9, and 10 are similar to curve 2, and indicate the BSBW being an along-slope gravity flow. Curve 11, being similar to curve 6 in Fig. 8c, corresponds to the θ - S indices of the UPDW. However, the BSBW is not observed in the section 126°E: see Fig. 8e, where a bunch of θ - S
360 curves (curves 12) presents all CTD profiles in the depth range 500–1200 m measured at the section 126°E of NABOS-09. Also we do not observe the BSBW further to the east on the section 142°E of NABOS-09 (not shown) as well as in the Makarov Basin.

To estimate the potential density of deep waters at the sections 103°E and 126°E σ_θ - S diagrams are shown in Fig. 8f: curves 2, 9 and 10 correspond to θ - S curves 2, 9 and 10 presented in Fig. 8d,
365 curves 12 correspond to curves 12 in Fig. 8e. As one can see, the BSBW is characterized by knee-shape diagram also in coordinates σ_θ , S . However the knee-shape diagram is not observed along 126°E in these coordinates. The dense and cold deep waters in the section 126°E have σ_θ , θ , S indices typical for the “true” BSBW mode (see paper by Dmitrenko et al. (2015)). Nevertheless, it is hardly correct to consider these waters (see σ_θ , S indices inside the circle; Fig. 8f) as the true BSBW mode, since σ_θ , θ , S
370 indices of these waters satisfactorily correspond to σ_θ , θ , S indices of the UPDW in the western part of the Nansen Basin (at longitudes to the west of 90°E). To evaluate the transformation of the “true” mode of the moving along the slope BSBW an additional analysis is required, which is beyond the scope of this paper.

Thus, the results presented in Fig. 8 show that the BSBW, which is characterized by the knee-shape diagram in coordinates θ , S and σ_θ , S , does not reach 126°E. This confirms the conclusions formulated in Subsection 3.1.1. Moreover, given the characteristic feature of the θ - S structure of BSBW in the St. Anna and Voronin Troughs (curves 1–4 in Fig. 8a) was observed in other years, we carried

out similar analysis using all available CTD data, which also confirmed the above conclusion. Thus, a
reasonable assumption, which could be made about the movement of BSBW over long distances in the
form of an along-slope gravity flow, is not confirmed by the analysis of a large volume of empirical
data.

According to (Schauer et al., 1997), the FSBW and BSBW merge and mix around 126°E and then
spread along the slope as a single flow. Thus, the question of transformation of the BSBW will remain
open. The absence of such waters at 126°E and further to the east along the slope can be considered a
kind of phenomenon. Indeed, let us compare Fig. 8d with Fig. 9, where the corresponding vertical
temperature profiles are presented (see the numbering of the θ - S curves and profiles).

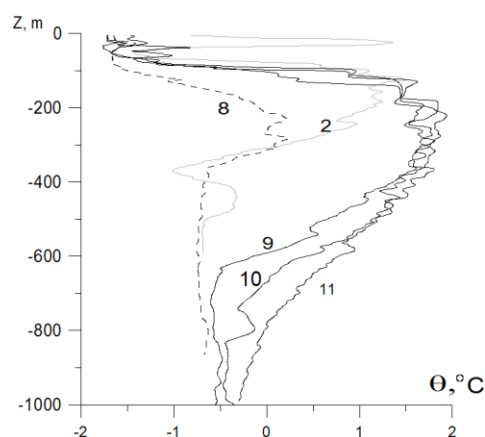


Fig. 9. Vertical temperature profiles from CTD-stations along 103°E (NABOS-09): curve 8 (st.64),
curve 9 (st. 63), curve 10 (st. 62), curve 11 (st. 60) (see the numbering of the θ - S curves in Fig. 8d) and
CTD-station across St. Anna Trough (NABOS-09, section 82°N), curve 2 (st.82).

The θ - S curves 2 and 10 in Fig. 8 correspond to vertical temperature profiles 2 and 10 in Fig. 9 for
the depth ranges of 300–600 m and 600–1000 m, respectively. The transformation of the profiles
evidences for an effect of stretching of the water column coming from the St. Anna Trough to the
Nansen Basin. This effect is described in detail in (Schauer et al., 1997).

Obviously, the movement of the BSBW along the slope does not occur adiabatically, so the
prominent knee-like feature (curve 2 in Fig.8a) corresponds to anomaly on profile 2 of Fig. 9 (below
300 m) should noticeably smooth out in the moving water mass. Nevertheless, it is possible to estimate

the cross section area ΔS through which the BSBW passes in the section along 103°E . Taking into
400 account the distance between stations at which profiles 9–11 were measured, we get $\Delta S \approx 2 \cdot 10^7 \text{ m}^2$.
Such a cross section area is not small: at an average cross-sectional flow velocity of 1 cm/s, the volume
flow rate through a cross section of this magnitude can reach about 0.2 Sv.

The absence of the main part of BSBW (with temperature less than -0.5°C) at longitudes to the
east of 126°E may be due to various reasons, including mixing with the FSBW caused by thermohaline
405 intrusive layering at stable-stable stratification (Merryfield, 2002; Kuzmina et al., 2013; Kuzmina et al.,
2014; Kuzmina, 2016, Zhurbas N., 2018; Kuzmina et al., 2018, 2019). Indeed, according to numerous
studies, the intrusive layering in the ocean determines the processes of exchange and mixing of various
water masses (see, e.g., Stern, 1967; Fedorov, 1976; Joyce, 1980; Zhurbas et al., 1993; Rudels et al.,
1999; Kuzmina, 2000; Walsh and Carmack, 2003). Other reasons for the missing main part of BSBW
410 may be the following: the influence of the slope topography, the impact of local counterflows near the
slope (a description of the counterflows is presented in (Pnyushkov et al., 2015)), lateral convection (a
discussion of the possibility of lateral convection occurrence in the near-slope zone can be found in e.g.
(Walsh et al., 2007), the observation and modelling of lateral convection are presented in (Ivanov and
Shapiro, 2005; Ivanov and Golovin, 2007)) and the impact of the Arctic Shelf Break Water (circulation
415 of the Arctic Shelf Break Water is investigated based on a numerical modeling (Aksenov et al.,
2011); the discussion on the influence of this branch on the process of mixing waters near the slope is
presented in (Ivanov and Aksenov, 2013)).

To clarify the reasons for the missing BSBW additional field measurements are required, namely,
CTD-transects across the slope between 103°E and 126°E .

420 **3.2 Characteristics of the Atlantic Water flow and geostrophic estimates of the volume flow rate**

Applying an approach described above in Section 2 the geostrophic estimates of the AW volume flow
rate V were calculated for all CTD transects available. These estimates of V , as well as estimates of the
hydrological parameters describing the AW flow in the Eurasian and Makarov Basins, are presented in
Table 1. The geostrophic estimates of the near-bottom gravity volume flow rate of the BSBW in zonal
425 transects across the St. Anna Trough are presented in Table 2. The only exception is the transect across



the St. Anna Trough at 82°N where the near-bottom gravity current is seen to have a considerable eastward constituent due to overflow across a sufficiently deep ridge (approx. 500 m deep) between the St. Anna Trough and the Voronin Trough. The presence of the eastward constituent of indefinite value makes questionable the results of geostrophic calculations only accounting for the northward constituent of the flow. Note also that prior to the BSBW entering the area of the Eurasian Basin, our estimates refer to the FSBW; to east of this region our estimates should be attributed to the joint contribution of two branches – the FSBW and BSBW – to the transfer of the AW.

The hydrological parameters shown in Table 1 can be interpreted as follows. The maximum water temperature of the AW may exceed 5 °C in cases when the AW inflow to the Eurasian Basin consists of especially warm water masses. A typical change in the maximum temperature of the moving along the continental slope AW over a distance of about 1000 km is approximately 1–2 °C. A typical change of the maximum salinity of the moving along the slope AW over the same distance does not exceed 0.1 psu. Such values of the maximum temperature of the AW lead to a slight increase in potential density and therefore a deviation of the AW from the isopycnic distribution should be expected. This effect is most likely associated with the exchange of heat, salt, and mass with the surrounding waters due to the formation of intrusive layering and the influence of double diffusion (on the observation and study of intrusions in the Arctic Basin see, e.g., Rudels et al., 1999; Kuzmina et al., 2011; Polyakov et al., 2012; Kuzmina et al., 2013). The intrusions and double diffusion that occurs at the boundaries of intrusions can also contribute to the reduction of the AW heat and salt content and the volume flow rate. The differences in the AW heat and salt content and the volume flow rate can be clearly seen from the PS-96 section when comparing data from stations near the continental slope of the Eurasian Basin at 92°E and from the vicinity of the Lomonosov Ridge at 140°E. It is worth noting that the maximum value of the AW temperature (θ_{max}) according to the presented data is always observed in the upper layer of the Eurasian Basin at the depths below the density jump layer but not exceeding 350 m, while the maximum salinity (S_{max}) at sections in the eastern part of the Basin can be observed at depths greater than 1000 m.

One of the key parameters in the analysis of flow dynamics, according to the authors, is the distance of the AW core (which can be associated with θ_{max}) from the slope/shelf boundary – $X_{\theta_{max}}$ in



455 Table 1. The highest value and the maximum variation of this parameter is observed near 126°E and
142°E, e.g. where the slope has a larger curvature (at about 126°E) or where the slope/shelf divides into
two “channels” (at about 142°E). Taking into account the dependence of the current dynamics in the
ocean on the bottom topography, the continental slope and the sea shelf, in these areas one can expect
the meandering of the current, and, as a result, the formation of intrusions and eddies, which, like the
intrusive layering, can have a significant effect on the AW heat and salt content and the volume flow
460 rate (the description of observation of eddies in the Eurasian Basin can be found in e.g. Schauer et al.,
2002; Dmitrenko et al., 2008; Aagaard et al., 2012).

A striking feature of the data is a noticeable increase of θ_{max} in 2006 at 31°E and 103°E. This
intensive warming of the AW was first reported in (Polyakov et. al., 2011). The present results show
that the increase of the temperature of the AW in 2006 was also accompanied by an increase of salinity
465 and volume flow rate of the geostrophic current (see the volume flow rate at the section along 103°E).
According to the authors, this can be caused not only by the warming of the AW, but also by an
increased inflow of the AW to the Eurasian Basin through the Fram Strait and St. Anna Trough.

Significant increase of the volume flow rate of the geostrophic current was observed in 2006: the
volume flow rate for the section at 103°E exceeds almost 5 times the value of the same parameter at the
470 same section assessed for the data of 2008. However, despite the anomalous conditions occurred in
2006, according to the data shown in the Table 1 it can be confidently concluded that in the process of
movement of the AW along the continental slope of the Eurasian Basin the volume flow rate of the
mean geostrophic flow gradually decreases. This fact is particularly well confirmed by the data
presented in Table 1 for 126–159°E: in this area the pattern of the spatial variability of the volume flow
475 rate does not change practically for 5 years. Thus a monotonous decrease in the volume flow rate is
observed with the AW moving away from the inflow zones.

Let us turn our attention to the following features of the volume flow rate estimates: high volume
flow rate estimates at 96°E, 103°E, 107°E, a negative volume flow rate estimate at 126°E in 2013 and
low volume flow rate estimates at 31°E, 60°E, 98°E in 2009 (Table 1). Indeed, the AW volume flow
480 rate in the BSBW area of entry into the Eurasian Basin in 2013 was almost equal to the maximum



485 volume flow rate in 2006 (103°E) and was quite high up to the longitude 107°E. This phenomenon as well as the intense warming in 2006 can be associated with the impact of climate conditions. The negative volume flow rate at 126°E was, according to the authors, due to the influence of local return flows which can be observed near the slope (Pnyushkov et al., 2015). Low FSBW volume flow rate estimates in 2009 are probably associated with a strong deviation of the flow from the slope, which may have been resulted in an underestimation of the AW volume flow rates due to the small length of the cuts to the north (see also below). Another reason may be a sharp decrease in the intensity of the flow of the AW through the Fram Strait that most likely took place that year.

490 It is also interesting to analyze the average values of volume flow rate V_{mean} for N transects available within a particular range of longitude/latitude. The mean values of the FSBW volume flow rate for the longitude range of 31–92°E is $V_{mean} = 0.44$ Sv for $N = 6$. This estimate of volume flow rate is about two times smaller than the estimate of the BSBW mean volume flow rate, $V_{mean} = 0.79$ Sv for $N = 3$ (see Table 2). The BSBW volume flow rate exceeding nearly twice the FSBW volume flow rate results in a dominance of the BSBW pattern of potential density contours in the longitude range of 94–107°E, where the both branches of the AW are present. Moreover, the sum of the mean values of the FSBW and the BSBW volume flow rate geostrophic estimates, $V_{mean} = (0.44 + 0.79) 10^6 = 1.23$ Sv, corresponds well to the mean geostrophic estimate of volume flow rate for the combined FSBW and BSBW flow within the range 94–107°E: $V_{mean} = 1.09$ Sv.

500 At the section 142°E located at the Lomonosov Ridge between the Amundsen and Makarov Basins, the geostrophic estimate of the along-slope volume flow rate of mixed waters of the FSBW and the BSBW reduces to $V_{mean} = 0.28$ Sv for $N = 9$ versus $V_{mean} = 0.39$ Sv for $N = 10$ at the section 126°E. Most likely the reduction is caused by splitting the AW flow into two flows, one of which goes further east along the slope in the Makarov Basin, and the second turns north along the Lomonosov Ridge to close cyclonic gyring of the AW around the Nansen and Amundsen Basins (Rudels et al., 2015).

505 Finally, at the section 159°E located in the Makarov Basin, the geostrophic estimate of the along-slope volume flow rate of mixed waters of the FSBW and the BSBW has further greatly reduced down



to $V_{mean} = 0.026$ Sv for $N = 2$, which is of more than one order of magnitude smaller than that in the Nansen and Amundsen Basins. Despite the low statistical significance of the latter estimate (due to small value of $N = 2$) one may conclude that the major part of the AW entering the Arctic Ocean circulates cyclonically within the Nansen and Amundsen Basins, and only its small part flows to the Makarov Basin (Rudels et al., 2015; Rudels, 2015). However, additional studies using more CTD data are required to confirm this result.

For the conclusion of the section, let us compare the estimates of volume flow rate presented in Table 1 with the estimates in other works. Based on the measurements of current velocities in the area of the West Spitsbergen Current near the Fram Strait, it was found that approximately 3 Sv of the AW flow into the Arctic Basin (Beszczynska-Möller et. al., 2012). These waters of Atlantic origin are divided into three "branches", one of which enters the Barents Sea, the other flows through the Fram Strait into the Nansen Basin, and the third branch recycles, reverses direction and approaches the West Greenland Current. The volume flow rate of the total AW flow, which enters the Barents Sea and the Nansen Basin, does not exceed 2–2.5 Sv, and therefore, taking into account the relaxation of the AW as it moves in the Arctic Basin, the total volume flow rate of the FSBW and BSBW in the Eurasian Basin can be close to 2 Sv. The same estimate, 2 Sv, for the sum of the FSBW and BSBW is suggested in (Rudels et. al., 1994). According to our calculations, the total volume flow rate of the FSBW and BSBW equal to 2.23 Sv was obtained only in 2006, when a strong warming of the AW was observed. Hence it cannot be excluded that the assessments obtained in this paper may in some cases be somewhat underestimated. According to the authors, this may be due to the fact that the sections along the longitudes 31°E and 103°E (see Fig. 1) are no longer than 100 km, and their vertical scale is only 1000 m. Actually, at the section along the longitude 31°E (Fig. 2, upper panel) only a part of the FSBW is observed, and at the section along the longitude 103°E (Fig. 2, lower panel) only the upper area of the BSBW is recorded. Therefore, it is reasonable to assume that the estimates obtained characterize, in some cases, the volume flow rates of the FSBW and BSBW in the areas, where the velocities have maximum values. Indeed, estimating the average velocities as $\bar{U} = V/S$ (where S is the area of the cross section, which was used to calculate the volume flow rate) we get about 1.5 cm/s in the first case (Fig.



2, upper panel), and about 4.5 cm/s in the second case (Fig. 2, lower panel). These are rather high values
 535 for the average velocities in the intermediate layer of the Nansen Basin (see, e.g., Aagaard, 1981).

Table 1. Characteristics of the Atlantic Water flow in the course of its propagation along continental
 slope of the Eurasian Basin of the Arctic Ocean. *Dist* is the along-slope distance from the Fram Strait;
 θ_{max} is the maximum temperature; $\sigma_{\theta}(Z_{\theta_{max}})$, $S(Z_{\theta_{max}})$, $Z_{\theta_{max}}$, and $X_{\theta_{max}}$ are the values of potential density,
 salinity, depth, and lateral displacement from the slope for the point θ_{max} ; S_{max} and $Z_{S_{max}}$ are the same as
 540 θ_{max} and $Z_{\theta_{max}}$ but for the salinity; V is the geostrophic estimate of the volume flow rate. The last row in
 the Table presents the characteristics of the return flow of the AW by the Lomonosov Ridge at the
 longitude 140°E and latitude 86.5°N (PS-96, see Fig. 1).

<i>Exp</i>	<i>Lon</i> [°E]	<i>Dist</i> [km]	θ_{max} [°C]	$\sigma_{\theta}(Z_{\theta_{max}})$ [kg/m ³]	$S(Z_{\theta_{max}})$ [psu]	$Z_{\theta_{max}}$ [m]	$X_{\theta_{max}}$ [km]	S_{max} [psu]	$Z_{S_{max}}$ [m]	V [Sv]
NABOS-06	31	404	5.670	27.579	34.980	42.0	-11	35.099	72.0	0.567
NABOS-08	31	404	4.883	27.771	35.103	101.5	0	35.105	175.5	0.801
NABOS-09	31	404	3.691	27.818	34.999	89.0	0	35.002	91.0	0.095
NABOS-09	60	856	2.503	27.891	34.951	175.0	10	34.981	362.5	0.128
NABOS-13	90	1290	2.600	27.903	34.975	250.0	41	34.996	333.0	0.464
PS-96	92	1322	2.786	27.875	34.960	271.0	33	34.968	329.0	0.583
NABOS-15	94	1355	2.445	27.946	35.012	331.0	33	35.015	365.0	0.472
NABOS-13	96	1388	2.548	27.902	34.969	207.0	70	34.978	264.0	2.059
NABOS-09	98	1421	2.300	27.906	34.948	220.5	79	34.971	344.5	0.088
NABOS-05	103	1561	2.029	27.870	34.876	179.5	39	34.934	308.5	0.317
NABOS-06	103	1561	2.528	27.888	34.950	220.0	50	34.978	260.0	2.228
NABOS-08	103	1561	1.980	27.886	34.891	201.5	60	34.929	325.0	0.417
NABOS-09	103	1561	1.984	27.913	34.925	244.5	50	34.951	364.5	0.872
NABOS-13	103	1561	2.278	27.904	34.942	215.0	80	34.956	419.0	1.587
NABOS-13	107	1695	1.903	27.937	34.945	359.0	120	34.948	404.0	1.774
NABOS-02	126	2104	1.406	27.938	34.902	324.0	243	34.932	2061.0	0.052
NABOS-03	126	2102	1.341	27.941	34.899	336.0	342	34.921	1886.0	0.413
NABOS-04	126	2102	1.770	27.906	34.896	271.0	87	34.925	2431.0	0.611
NABOS-05	126	2102	1.695	27.936	34.926	359.0	227	34.935	2841.0	0.754
NABOS-06	126	2102	1.905	27.923	34.930	284.0	193	34.960	968.0	0.774
NABOS-07	126	2102	2.085	27.907	34.928	266.0	242	34.942	340.0	0.600
NABOS-08	126	2102	2.195	27.885	34.911	206.0	235	34.939	365.0	0.310
NABOS-09	126	2102	1.907	27.909	34.913	316.5	33	34.932	1018.0	0.404
NABOS-13	126	2102	1.946	27.937	34.949	346.0	228	34.951	428.0	-0.209
NABOS-15	126	2102	1.653	27.918	34.898	246.0	400	34.942	3816.0	0.224
NABOS-03	142	2456	1.089	27.912	34.841	269.0	41	34.862	1000.0	0.063
NABOS-04	142	2456	1.401	27.909	34.865	281.0	0	34.907	1608.0	0.209
NABOS-05	142	2456	1.492	27.906	34.870	284.0	100.0	34.906	1550.0	0.264
NABOS-06	142	2456	1.981	27.874	34.876	234.0	111.0	34.960	1016.0	0.603



NABOS-07	142	2456	1.855	27.879	34.870	231.0	0.0	34.920	2064.0	0.087
NABOS-08	142	2456	1.599	27.915	34.890	260.5	200.0	34.908	347.0	0.226
NABOS-09	142	2456	1.704	27.915	34.900	253.5	101.0	34.917	1082.0	0.215
NABOS-13	142	2456	1.475	27.940	34.909	331.0	115.0	34.926	1150.0	0.181
NABOS-15	142	2456	1.353	27.936	34.892	326.0	106.0	34.913	1372.0	0.633
NABOS-07	159	2783	1.424	27.887	34.839	255.0	0.0	34.880	1075.0	-0.006
NABOS-08	159	2783	1.383	27.893	34.843	245.0	0.0	34.889	1265.5	0.058
PS-96back	140E 86.5N	3178	1.812	27.890	34.880	219.0	≈ 700	34.902	472.0	-0.088

Table 2. Geostrophic estimates of the volume flow rate for near-bottom gravity flow of the Barents Sea Branch of Atlantic Water (BSBW) on zonal transects across the St. Anna Trough.

<i>Exp</i>	NABOS-09	NABOS-13	NABOS-15
<i>Lat</i> [°N]	81.00	81.33	81.41
<i>V</i> [Sv]	0.892	0.727	0.755

545

3.3 Inter-annual variability of the AW temperature-salinity indices and the volume flow rate

Within the NABOS project, in accordance with Table 1, the cross-slope CTD transects at 103°E, 126°E, and 142°E were repeatedly performed for a number of annual campaigns: 2005, 2006, 2008 and 2013 (103°E), 2002–2009, 2013 and 2015 (126°E), 2003–2009, 2013, and 2015 (142°E). The repeated transects may contain some information on inter-annual variability of the AW, and we attempted to explore such a possibility.

550

Time series of the maximum temperature of the AW, θ_{max} , and the related values of salinity $S(\theta_{max})$ and potential density anomaly $\sigma_{\theta}(\theta_{max})$ (Fig. 10) show that the period of 2006–2008 was characterized by an increased temperature of the AW in the eastern part of the Eurasian Basin. The temperature excess during this period was as large as about 0.6–1.0 °C relative to the years 2002–2003 and 0.3–0.6 °C relative to the years 2013–2015. During the whole NABOS period 2002–2015, the AW temperature in the eastern part of the Eurasian Basin had slightly increased by 0.2–0.3 °C. The time series of corresponding values of salinity $S(\theta_{max})$ displayed in 2006 local maxima at the transects 126°E and 142°E, and the absolute maximum at the transect 103°E; the salinity excess for the maxima largely decreased with the longitude from approximately 0.06 psu at 103°E to less than 0.01 psu at 142°E. Note, that the time series of θ_{max} had the absolute maximum in 2006–2008 that can be interpreted as a

555

560



565 result of heat impulse of the early 2000-ies (Polyakov et al., 2011). In accordance with our analysis the time series of θ_{max} had a maximum in 2013 but only at 103°E (see Table 1 and Fig.10). The time series of $S(\theta_{max})$ display an increase of AW salinity in 2006–2008 and 2013 also, that can be referred to as a AW salinization in early 2000-ies. The change of salinity of AW at 142°E in time also draws attention to the following aspects: the salinity increases almost monotonously in the period from 2003 to 2013. How can such behavior of salinity be explained is not clear. It is also worth noting that the maxima of θ_{max} and $S(\theta_{max})$ in 2006-2008 and 2013 (at 103°E) were accompanied by the volume flow rate highs.

4 Summary

570 The estimates of θ - S indices and of the volume flow rate of the current carrying the AW in the Eurasian Basin were obtained. The estimates were based on the analysis of CTD data collected within the NABOS program in 2002–2015 including 33 transects in the Eurasian Basin, 2 transects in the Makarov Basin and 4 transects in the St. Anna Trough; additionally CTD transect PS-96 was considered.

575 First of all, the variability of the thermohaline pattern on the AW pathway along the slope of the Eurasian Basin was investigated. It was found that the FSBW was satisfactorily identified at all transects, including the two transects in the Makarov Basin (159°E), while the cold waters at the transects along longitudes 126°E, 142°E and 159°E, which can be associated with the influence of the BSBW, were observed in the depth range below 800 m and had little effect on the spatial structure of isopycnic surfaces. To study the transformation of the moving along the slope BSBW the θ - S analysis was applied. It was shown, that the BSBW, which is characterized by the knee-shape diagram in coordinates θ , S and σ_θ , S (see Fig.8), does not reach the longitude 126°E. Thus, a reasonable assumption, which could be made about the movement of the BSBW over long distances in the form of along-slope gravity flow, is not confirmed by the analysis of a large amount of empirical data. To
580 clarify the reasons for the BSBW missing at 126°E and to the east of the slope additional field measurements are required, namely, CTD transects across the slope between the longitudes 103°E and
585 126°E.



A special attention was paid to the study of the variability of the volume flow rate of the AW propagating along the continental slope of the Eurasian Basin. The volume flow rate of the geostrophic flow was calculated using the dynamic method. The estimates are given in tabular form. An interpretation of the spatial and temporal variability of hydrological parameters characterizing the flow of the AW in the Eurasian Basin is presented.

The performed analysis showed that the geostrophic volume flow rate decreases significantly farther away from areas of the AW inflow in the Eurasian Basin. This decrease may be primarily due to a decrease of the flow velocity. Thus, on the basis of direct velocity measurements, it was shown that the mean velocity of the current along the continental slope gradually decreases (Pnyushkov et al., 2015). Another reason is the weakening of the horizontal gradients of potential density caused by the advection of water masses in the direction perpendicular to the eastward geostrophic flow. Such advection can be attributed to the processes of formation of intrusions and eddies, which are typically observed in the intermediate and deep layers of the Eurasian Basin.

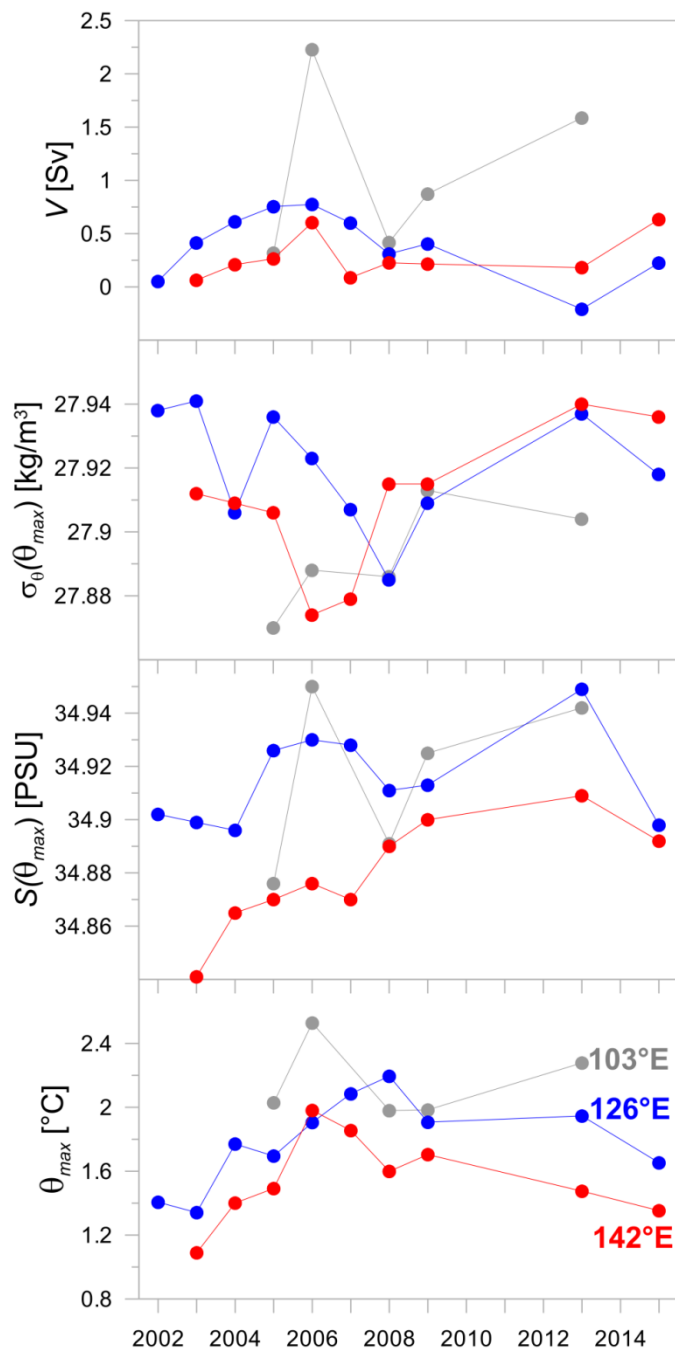
A study of the temporal variability of hydrological parameters and of the volume flow rate is summarized as follows. The time series of θ_{max} had an absolute maximum in 2006–2008 that can be interpreted as a result of heat impulse in the early 2000-ies (Polyakov et al., 2011). In accordance with our analysis the time series of θ_{max} had a maximum in 2013 but only at the longitude 103°E (see also Table 1 and Fig.10). The time series of $S(\theta_{max})$ also display an increase of AW salinity in 2006–2008 and 2013, that can be referred to as a AW salinization in the early 2000-ies. The change of salinity of AW at 142°E in time also draws attention to the following aspect: the salinity increases almost monotonously in the period from 2003 to 2013. How can such behavior of salinity be explained is not clear. It is important to underline also that the maxima of θ_{max} and $S(\theta_{max})$ in 2006–2008 and 2013 (103°E) were accompanied by the volume flow rate highs.

A comparison of the presented results with the results obtained in the well-known paper (Rudels et al., 2015) reveals some differences in interpretation. It was suggested in (Rudels et al., 2015) that the BSBW supplies the major part of the AW to the Amundsen, Makarov and Canadian Basins, while the FSBW remains almost fully in the Nansen Basin. The analysis of the data performed in the present



615 work showed that the thermohaline structure of the water masses in the region east of the inflow of the
BSBW in the Nansen Basin (at around 103°E) is more complicated due to the interaction between the
two branches of the AW. Large slopes of isopycnic surfaces on the horizons below 800 m (the depth
range of the BSBW) and intense perturbations of the density field typical of eddy structures are
observed on the transects in this area. However, already at 142°E the core of the directed to the east
620 geostrophic current is located in the upper active layer and the θ - S indices of waters in the current area
correspond to the FSBW. Thus, there is a certain paradox: on the one hand, the mean geostrophic
volume flow rate of BSBW is higher than the mean volume flow rate of FSBW (see Section 3.2), and
on the other hand, the BSBW, which is characterized by the knee-shape diagram in coordinates θ , S and
 σ_θ , S , does not reach 126°E. It should also be emphasized that the weak geostrophic current in the
625 Makarov Basin at 159°E is confined to the upper active layer (up to 500 m), and the thermohaline
characteristics of the flow also correspond to the θ - S indices of the FSBW. Taking into account that the
volume flow rate values in the Makarov Basin are much smaller than the volume flow rate values found
in the Eurasian Basin, it can be concluded that the major part of the AW entering the Nansen Basin (and
not only the FSBW) remains in the Eurasian Basin, and only a small part of the AW enters the Makarov
630 and Canadian Basin. Exceptions may arise when strong inflows of the BSBW into the Nansen Basin
occur due to the influence of sharp climatic changes on the thermohaline structure of waters in the
central part of the Arctic Ocean.

This study is a natural step in the research of the spatial and temporal variability of the
geostrophic current carrying the AW along the continental slope of the Eurasian Basin. The table of
635 hydrological parameters presented in the paper may be used as a required reference material for
comparative estimates of the variability amplitudes of the θ - S indices arising from climate change in the
Arctic Basin. The continuation of similar studies based on new CTD data from the NABOS program
can facilitate answering the addressed in this study important questions about the transformation and
advection of the AW.



640

Fig. 10. Interannual variability of the maximum temperature θ_{max} and the related values of salinity $S(\theta_{max})$, potential density anomaly $\sigma_{\theta}(\theta_{max})$ and volume flow rate V on the cross-slope transects at 103°E, 126°E and 142°E.



Acknowledgments. This research, including the approach development, data processing and
645 interpretation, performed by Nataliya Zhurbas, was funded by Russian Science Foundation, project no.
17-77-10080. Natalia Kuzmina (θ - S analysis, participation in discussion) was supported by the state
assignment of the Shirshov Institute of Oceanology RAS (theme no. 0149-2019-0003).

References

- Aagaard, K.: On the deep circulation of the Arctic Ocean, *Deep-Sea Res.*, 28, 251–268, 1981.
- 650 Aagaard, K., Andersen, R., Swift, J., and Johnson, J.: A large eddy in the central Arctic Ocean,
Geophys. Res. Lett., 35, L09601, doi: 10.1029/2008GL033461, 2008.
- Aksenov, Y., Ivanov, V. V., Nurser, A. J. G., Bacon, S., Polyakov, I. V., Coward, A. C., Naveira-
Garabato, A. C., and Beszczynska-Moeller, A.: The Arctic Circumpolar Boundary Current, *J.*
Geophys. Res., 116, C09017, 1–28, doi:10.1029/2010JC006637, 2011.
- 655 Arneborg, L., Fiekas, V., Umlauf, L., and Burchard, H.: Gravity current dynamics and entrainment – A
process study based on observations in the Arkona Basin, *J. Phys. Oceanogr.*, 37, 2094–2113,
doi:10.1175/JPO3110.1, 2007.
- Beszczynska-Möller, A., Fahrbach, E., Schauer, U., and Hansen, E.: Variability in Atlantic water
temperature and transport at the entrance to the Arctic Ocean, 1997–2010, *ICES Journal of Marine*
660 *Science*, 69(5), 852–863, doi: 10.1093/icesjms/fss056, 2012.
- Dmitrenko, I. A., Kirillov, S. A., Ivanov, V. I., and Woodgate, R.: Mesoscale Atlantic water eddy off
the Laptev Sea continental slope carries the signature of upstream interaction, *J. Geophys. Res.*, 113,
C07005, doi: 10.1029/2007JC004491, 2008.
- Dmitrenko, I. A., Rudels, B., Kirillov, S. A., Aksenov, Y. O., Lien V. S., Ivanov, V. V., Schauer, U.,
665 Polyakov, I. V., Coward, A., and Barber, D. J.: Atlantic Water flow into the Arctic Ocean through
the St. Anna Trough in the northern Kara Sea, *J. Geophys. Res.: Oceans*, 120(7), 5158–5178, doi:
10.1002/2015JC010804, 2015.
- Fahrbach, E., Meincke, J., Osterhus, S., Rohardt, G., Schauer, U., Tverberg, V., and Verduin, J.: Direct
measurements of volume transport through Fram Strait, *Polar Res.*, 20(2), 217–224, doi:
670 10.1111/j.1751-8369.2001.tb00059.x, 2001.



- Fedorov, K. N.: Physical Nature and Structure of Oceanic Fronts, Gidrometeoizdat, Leningrad, 296 pp., 1983 (in Russian).
- Ivanov, V. V., and Shapiro, G. I.: Formation of dense water cascade in the marginal ice zone in the Barents Sea, *Deep-Sea Res. I*, 52, 1699–1717, doi: 10.1016/j.dsr.2005.04.004, 2005.
- 675 Ivanov, V., and Golovin, P.: Observations and modelling of dense water cascading from northwestern Laptev Sea shelf, *J. Geophys. Res.*, 112, C09003, doi:10.1029/2006JC003882, 2007.
- Ivanov, V. V., and Aksenov, E. O.: Atlantic Water transformation in the Eastern Nansen Basin: observations and modelling, *Arctic and Antarctic Research*, 1(95), 72–87, 2013 (in Russian).
- Joyce, T. M.: A note on the lateral mixing of water masses, *J. Phys. Oceanogr.*, 7(4), 626–629, 1980.
- 680 Kuzmina, N. P.: On the parameterization of interleaving and turbulent mixing using CTD data from the Azores Frontal Zone, *J. Mar. Syst.*, 23(4), 285–302, 2000.
- Kuzmina, N., Rudels, B., Zhurbas, V., and Stipa, T.: On the structure and dynamical features of intrusive layering in the Eurasian Basin in the Arctic Ocean, *J. Geophys. Res.*, 116, C00D11, doi: 10.1029/2010JC006920, 2011.
- 685 Kuzmina, N. P., Zhurbas, N. V., and Rudels B.: Structure of intrusions and fronts in the deep layer of the Eurasian Basin and Makarov Basin (Arctic), *Oceanology*, 53(4), 410–421, doi: 10.1134/S0001437013040061, 2013.
- Kuzmina, N. P., Zhurbas, N. V., Emelianov, M. V., and Pyzhevich, M. L.: Application of interleaving Models for the Description of intrusive Layering at the Fronts of Deep Polar Water in the Eurasian Basin (Arctic), *Oceanology*, 54(5), 557–566, doi: 10.1134/S0001437014050105, 2014.
- 690 Kuzmina, N. P.: Generation of large-scale intrusions at baroclinic fronts: an analytical consideration with a reference to the Arctic Ocean, *Ocean Sci.*, 12, 1269–1277, doi: 10.5194/os-12-1269-2016, 2016.
- Kuzmina, N. P., Skorokhodov, S. L., Zhurbas, N. V., and Lyzhkov, D. A.: On instability of geostrophic current with linear vertical shear at length scales of interleaving, *Izv. Atmos. Ocean. Phys.*, 54(1), 47–55, doi: 10.1134/S0001433818010097, 2018.
- 695 Merryfield, W. J.: Intrusions in Double-Diffusively Stable Arctic Waters: Evidence for Differential mixing?, *J. Phys. Oceanogr.*, 32, 1452–1459, 2002.



- Pfirman, S.L., Bauch, D, and Gammersrod, T.: The northern Barents Sea: water mass distribution and
700 modification., in *The Polar Oceans and Their Role in Shaping the Global Enviroment*, O.M.
Johannessen, R.D. Muench, and J.E. Overland, eds., American Geophysical Union, Geophysical
Monograph 85, 77-94.
- Pnyushkov, A. V., Polyakov, I. V., Ivanov, V. V., Aksenov, Ye., Coward, A., Janout, M., and Rabe, B.:
Structure and variability of the boundary current in the Eurasian Basin of the Arctic Ocean, *Deep-*
705 *Sea Res. I*, 101, 80–97, doi: 10.1016/j.dsr.2015.03.001, 2015.
- Polyakov, I. V., Beszczynska, A., Carmack, E. C., Dmitrenko, I. A., Fahrbach, E., Frolov, I. E., Gerdes,
R., Hansen, E., Holfort, J., Ivanov, V. V., Johnson, M. A., Karcher, M., Kauker, F., Morison, J.,
Orvik, K. A., Schauer, U., Simmons, H. L., Skagseth, Ø., Sokolov, V. T., Steele, M., Timokhov, L.
A., Walsh, D., and Walsh, J. E.: One more step toward a warmer Arctic, *Geophys. Res. Lett.*, 32,
710 L17605, doi: 10.1029/2005GL023740, 2005.
- Polyakov, I. V., Alexeev, V. A., Ashik, I. M., Bacon, S., Beszczynska-Möller, A., Carmack, E. C.,
Dmitrenko, I. A., Fortier, L., Gascard, J.-C., Hansen, E., Hölemann, J., Ivanov, V. V., Kikuchi, T.,
Kirillov, S., Lenn, Y.-D., McLaughlin, F. A., Piechura, J., Repina, I., Timokhov, L. A., Walczowski,
W., and Woodgate, R.: Fate of Early 2000s Arctic Warm Water Pulse, *Bulletin of the American*
715 *Meteorological Society*, 92(5), 561–566, doi: 10.1175/2010BAMS2921.1, 2011.
- Polyakov, I. V., Pnyushkov, A., Rember, R., Ivanov, V., Lenn, Y-D., Padman, L., and Carmack, E. C.:
Mooring-based observations of the double-diffusive staircases over the Laptev Sea, *J. Phys.*
Oceanogr., 42, 95–109, doi: 10.1175/2011JPO4606.1, 2012.
- Rudels, B., Jones, E. P., Anderson, L. G., and Kattner, G.: On the intermediate depth waters of the
720 Arctic Ocean, in: *The Role of the Polar Oceans in Shaping the Global Climate*, edited by:
Johannessen, O. M., Muench, R. D., and Overland, J. E., American Geophysical Union, Washington,
DC, 33–46, 1994.
- Rudels, B., Björk, G., Muench, R. D, and Schauer, U.: Double-diffusive layering in the Eurasian Basin
of the Arctic Ocean, *J. Mar. Syst.*, 21(1–4), 3–27, doi: 10.1016/S0924-7963(99)00003-2, 1999.
- 725 Rudels, B., Jones, E. P., Schauer, U., and Eriksson, P.: Atlantic sources of the Arctic Ocean surface and
halocline water, *Polar research*, 23(2), 181–208, doi: 10.1111/j.1751-8369.2004.tb00007.x, 2006.



- Rudels, B., Kuzmina, N., Schauer, U., Stipa, T., and Zhurbas, V.: Double-diffusive convection and interleaving in the Arctic Ocean – Distribution and importance, *Geophysica*, 45(1–2), 199–213, 2009.
- 730 Rudels, B.: Arctic Ocean circulation, processes and water masses: A description of observations and ideas with focus on the period prior to the International Polar Year 2007–2009, *Progress in Oceanography*, 132, 22–67, doi: 10.1016/j.pocean.2013.11.006, 2015.
- Rudels, B., Korhonen, M., Schauer, U., Pisarev, S., Rabe, B., and Wisotzki A.: Circulation and transformation of Atlantic water in the Eurasian Basin and the contribution of the Fram Strait inflow branch to the Arctic Ocean heat budget, *Progress in Oceanography*, 132, 128–152, doi: 735 10.1016/j.pocean.2014.04.003, 2015.
- Schauer, U., Muench, R. D., Rudels, B., and Timokhov, L.: Impact of eastern Arctic shelf waters on the Nansen Basin intermediate layers, *J.Geophysical Res.*, 102(C2), 3371–3382, 1997.
- Schauer, U., Rudels, B., Jones, E. P., Anderson, L. G., Muench, R. D., Björk, G., Swift, J. H., Ivanov, 740 V., and Larsson, A.-M.: Confluence and redistribution of Atlantic water in the Nansen, Amundsen and Makarov basins, *Ann. Geophys.*, 20, 257–273, doi: 10.5194/angeo-20-257-2002, 2002.
- Stern, M. E.: Lateral mixing of water masses, *Deep-Sea Res.*, 14, 747–753, doi:10.1016/S0011-7471(67)80011-1, 1967.
- Walsh, D., and Carmack, E.: The nested structure of Arctic thermohaline intrusions, *Ocean Model.*, 5, 745 267–289, doi: 10.1016/S1463-5003(02)00056-2, 2003.
- Walsh D., Polyakov I., Timokhov L., and Carmack E.: Thermohaline structure and variability in the eastern Nansen Basin as seen from historical data, *Journal of Marine Research*, 65, 685–714, 2007.
- Zhurbas, N. V.: On the eigenvalue spectra for a model problem describing formation of the large-scale intrusions in the Arctic Basin, *Fundamentalnaya I Prikladnaya Gidrofizika*, 11(1), 40–45, doi: 750 10.7868/S2073667318010045, 2018.
- Zhurbas, N. V.: Estimates of transport and heat content of the Atlantic Water while its propagation along the Eurasian Basin slope, *Russian Meteorology and Hydrology*, 2019 (Submitted).



755

Zhurbas, V. M., Kuzmina, N. P., Ozmidov, R. V., Golenko, N. N., and Paka, V. T.: Manifestation of subduction in thermohaline fields of vertical fine structure and horizontal mesostructure in frontal zone of Azores Current, *Okeanologiya+*, 33, 321–326, 1993.

Zhurbas, V., Elken, J., Paka, V., Piechura, J., Väli, G., Chubarenko, I., Golenko, N., and Shchuka, S.: Structure of unsteady overflow in the Słupsk Furrow of the Baltic Sea, *J. Geophys. Res. – Oceans*, 117, C04027, doi:10.1029/2011JC007284, 2012.